ABS Nanocomposite Films Based on Functionalized-Graphene Sheets

Cheol Heo,[1] Hyun-Gon Moon,[1] Choon Sup Yoon,[2] Jin-Hae Chang[1]

[1]*School of Energy and Integrated Materials Engineering, Kumoh National Institute of Technology, Gumi 730-701, Korea*
[2]*Department of Physics, KAIST, Daejeon 305-701, Korea*

Received 20 August 2010; accepted 29 July 2011
DOI 10.1002/app.35404
Published online 6 December 2011 in Wiley Online Library (wileyonlinelibrary.com).

ABSTRACT: Acrylonitrile-butadiene-styrene (ABS)/functionalized-graphene nanocomposites were synthesized using the solution-blending method in chloroform. A dispersion of graphite oxide was added to a solution of the ammonium salt of octadecylamine (C18) to form octadecylamine-graphene (C18-graphene), which was then used as a functionalized graphene in the preparation of ABS nanocomposite films. ABS nanocomposite films with different C18-graphene contents (0–3 wt %) were compared in terms of their thermomechanical properties and morphology. Despite the relatively low C18-graphene loadings studied, the nanocomposite films exhibited greatly improved thermomechanical properties compared with pure ABS. © 2011 Wiley Periodicals, Inc. J Appl Polym Sci 124: 4663–4670, 2012

Key words: functionalized graphene; graphene nanocomposite; octadecylamine-graphene

INTRODUCTION

Graphene, a two-dimensional carbon structure that exhibits remarkable electronic and mechanical properties, has great potential in material science for both fundamental research and technological applications.[1–3] Several methods of synthesizing graphene have been developed, such as the scotch-tape method,[4,5] epitaxial growth on a SiC wafer,[1,6] and chemical exfoliation.[7–9] The first two methods are unsuitable for producing graphene layers with high surface area in large quantities at low cost. The chemical method, which was initially developed by Stankovich et al.,[10] was used to fabricate solution-processable functionalized graphene in two stages. First, water-soluble graphite oxide (GO) was prepared from graphite using the Hummers method[11] and dispersed in water with appropriate sonication to yield a dispersion containing mainly individual graphene sheets. Second, the exfoliated GO was reacted with an alkylamine to obtain a solution-processable functionalized graphene. This procedure was followed in the present work.

Functionalization of the graphene surface is a method designed to introduce reactive moieties, to disrupt the bundle structure, and to potentially obtain individual sheets.[12,13] Functional moieties are attached to open ends and sidewalls, primarily to improve the solubility as well as the dispersibility of graphene sheets.

Here we describe the use of chemical functionalization of graphene, particularly alkylation, to address the problems of both dispersion and interaction between the graphene sheets and the matrix acrylonitrile-butadiene-styrene (ABS) polymer in chloroform. The thermomechanical properties and morphology of ABS-hybrid films containing functionalized graphene are compared to those of pure ABS. The effects of functionalized-graphene content on thermomechanical properties and morphology are also discussed.

EXPERIMENTAL

Materials

All reagents were purchased from Junsei Chemical (Tokyo, Japan) and Aldrich Chemical (Yongin, Korea). Commercially available solvents were purified by distillation. Common reagents were used without further purification. Natural flake graphite, particle size 75 mesh, was purchased from Aldrich Chemical (Yongin, Korea). ABS (HF 380) polymer was kindly provided by LG Chemical (Daejeon, Korea).

Correspondence to: J.-H. Chang (changjinhae@hanmail.net).

Contract grant sponsor: NRF, Ministry of Education, Science and Technology, Korea; contract grant number: 2009-0074072.

Preparation of functionalized graphene: C18-graphene

GO was synthesized from natural graphite via a multistep route known as Hummer's method.[11] Octadecylamine-graphene (C18-graphene) was synthesized from *n*-octadecylamine (C18) and GO, as follows. One gram (3.71 mmol) of C18 was added to 100 mL of ethanol. This mixture was stirred at room temperature under a steady stream of N_2 gas. One gram of GO was dissolved in 100 mL of distilled water and then this solution was added to the C18/ethanol system. The mixture was heated for 24 h at 100°C under a steady stream of N_2 gas. One gram of hydroquinone was added, and the mixture was refluxed for 22 h to remove excess C18. The reaction product was cooled to room temperature and repeatedly washed with water and ethanol for three times each, then dried under vacuum at 80°C for 1 day to obtain the C18-graphene.

Preparation of ABS/C18-graphene hybrid films

All of the ABS/C18-graphene film samples were prepared by the solution-intercalation method. The synthesis procedures for the hybrid films with various C18-graphene contents are very similar, so only a representative example, the procedure for the preparation of the nanocomposite containing 1 wt % C18-graphene, is described here. In a 100 mL beaker, 2 g of ABS and 30 mL of chloroform were placed; the mixture was stirred for 24 h at room temperature. In a separate beaker, 0.02 g of C18-graphene was ultrasonicated in chloroform for 10 h; this mixture was added to the ABS solution with vigorous stirring for 12 h at room temperature under a steady stream of N_2 gas, to obtain a homogeneously dispersed system. The resulting solution was cast onto glass plates under vacuum at 45°C for 24 h. The films were dried in a drying oven at 80°C for 24 h. The resulting film thickness of the hybrid films is 80–100 μm.

Characterization

Fourier transform infrared (FTIR) spectra were obtained with an FTIR 460 (JASCO) instrument in the range 4000–600 cm^{-1} using KBr pellets. Atomic force microscopy (AFM; Multimode, NanoScope III, Digital instruments) images were taken on an AutoProbe CP/MT scanning probe microscope. GO samples were dispersed in water, and C18-graphene samples in toluene. The suspensions were ultrasonicated for 3 h, and then spin-coated at 5000 rpm on silicon wafers. Wide-angle X-ray diffraction (XRD) measurements were performed at room temperature on a Rigaku (D/Max-IIIB) X-ray diffractometer using Ni-filtered Cu-Kα radiation. The scanning rate was 2°/min over the range $2\theta = 2°–32°$.

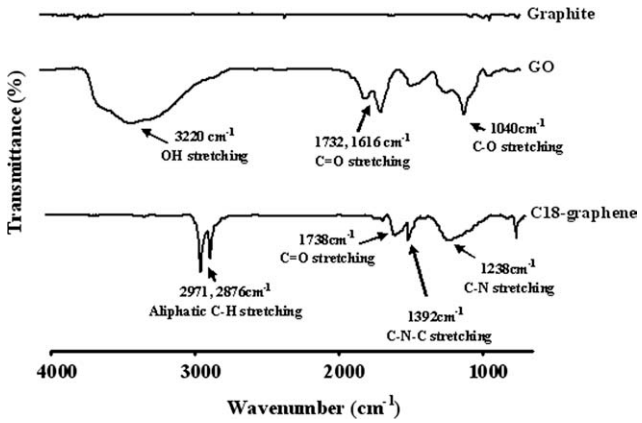

Figure 1 FTIR spectra of Graphite, GO, and C18-graphene.

The morphologies of the fractured surfaces of the extrusion samples were investigated using a Hitachi S-2400 scanning electron microscope (SEM). To enhance the conductivity, the fractured surfaces were sputter-coated with gold using an SPI Sputter Coater. Transmission electron microscope (TEM) micrographs of ultrathin sections of the ABS hybrid films were recorded using an EM 912 OMEGA TEM with an acceleration voltage of 120 kV.

Differential scanning calorimetry (NETZSCH F3) and thermogravimetric analysis (TGA, TA Q500) were performed at a heating rate of 20°C/min under an N_2 flow. The tensile properties of the solution-cast films were determined using an Instron Mechanical Tester (Model 5564) at a crosshead speed of 2 mm/min (ASTM D882). The specimens used in these tests were prepared by cutting strips with dimensions of 5 × 70 mm^2. At least 10 individual determinations were used to obtain an average value. The experimental uncertainties in the tensile strength and the modulus were ±1 MPa and ±0.05 GPa, respectively.

RESULT AND DISCUSSION

FTIR

Figure 1 shows the FTIR spectra of pure graphite, GO, and C18-graphene. The pure graphite shows no characteristic peak as shown in Figure 1. The GO spectrum contains strong, broad absorption peaks because of OH and COOH.

FTIR spectrum (KBr) of GO: 3220 cm^{-1} (OH), 1732 and 1616 cm^{-1} (C═O), and 1040 cm^{-1} (C─O).

FTIR spectrum (KBr) of C18-graphene: 2971 and 2876 cm^{-1} (aliphatic C─H), 1738 cm^{-1} (C═O), 1392 cm^{-1} (C─N─C), and 1238 cm^{-1} (C─N).

Morphology

The AFM results show that the carbon sheets obtained by our method are only a single atomic layer thick. A

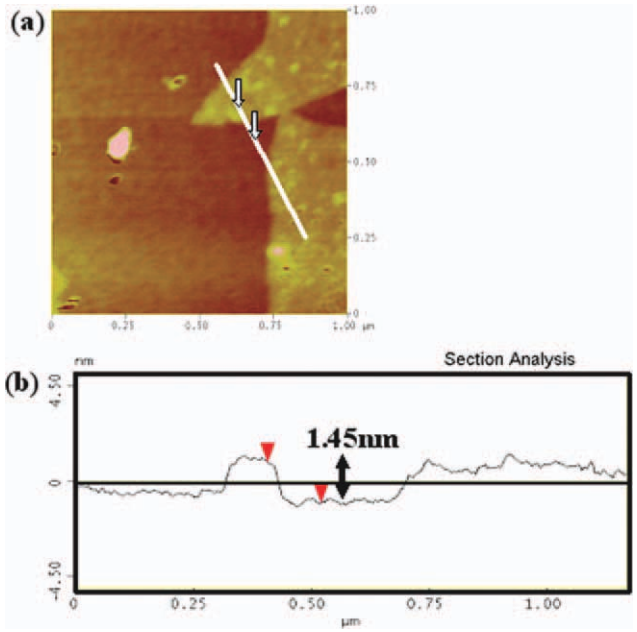

Figure 2 AFM image of GO (a) 2D image and (b) height of white arrow line in (a). [Color figure can be viewed in the online issue, which is available at wileyonlinelibrary.com.].

typical AFM image of GO sheets deposited onto a mica substrate from an aqueous dispersion is shown in Figure 2, with superimposed cross-section measurements taken along the white line indicating a sheet thickness of 1.45 nm (averaged over about 20 sheets). Aksay and coworkers[14] have previously reported on the average thickness of these graphene sheets. They also reported that the minimum sheet thickness is 1.1 nm, and the mean is 1.75 nm when the thicknesses of 140 sheets were measured.

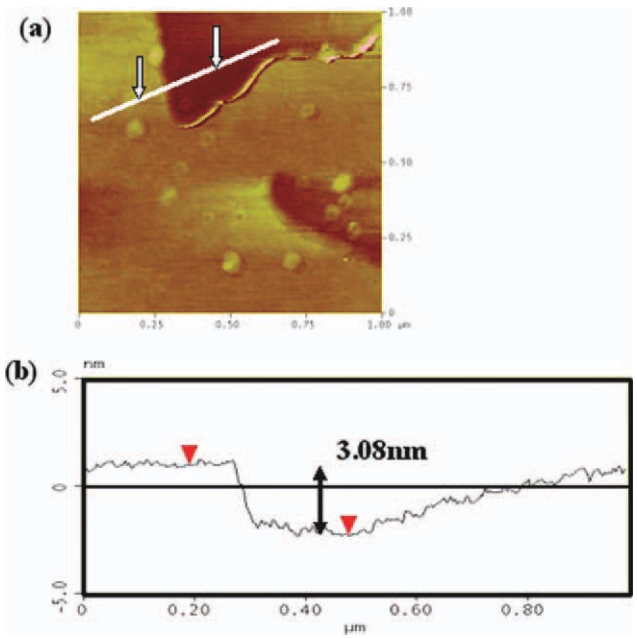

Figure 3 AFM images of C18-graphene (a) 2D image and (b) height of white arrow line in (a). [Color figure can be viewed in the online issue, which is available at wileyonlinelibrary.com.].

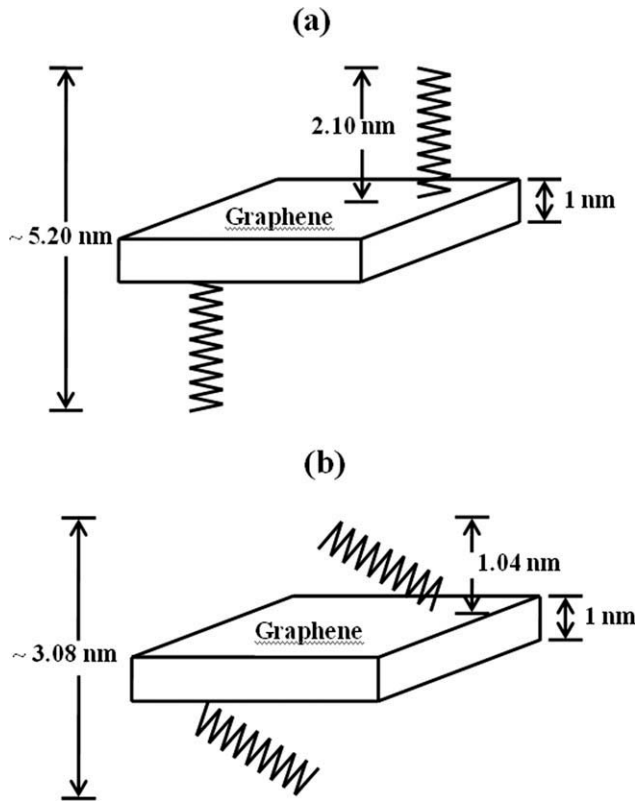

Figure 4 Formation of C18-graphene layers from GO and *n*-octadecylamine reagent: (a) theoretical values and (b) experimental values from AFM.

Figure 3 shows an AFM image of C18-treated GO (C18-graphene) sheets on mica, as well as a profile plot showing a sheet thickness of 3.08 nm. The theoretical thickness for a graphene sheet functionalized on both sides is $\sim$ 5.2 nm, assuming that the thickness of the bare graphene sheet is 1 nm, with the substituted long-alkyl (octadecylamine) groups contributing $\sim$ 2.1 nm in thickness.[15] On average, the thickness of these C18-graphene sheets is about 3 nm. The AFM micrograph in Figure 3(b) shows that the C18-graphene sheets are exfoliated, and the nanosheets may be composed of single graphene sheets.[10] Figure 4 shows a schematic diagram of the formation of C18-graphene sheets in hybrid films.

The dispersion of graphene sheets was further examined with XRD, which provides complementary data to the AFM results. The XRD patterns for pristine graphite, GO, and C18-graphene are illustrated in Figure 5. The d_{001} reflection for graphite is found at $2\theta = 26.6^\circ$, which corresponds to an interlayer distance of 3.35 Å. When the GO and C18-graphene are dispersed in water and chloroform, respectively, no obvious graphite peaks are observed, indicating that the graphite disperses homogeneously in each solvent.

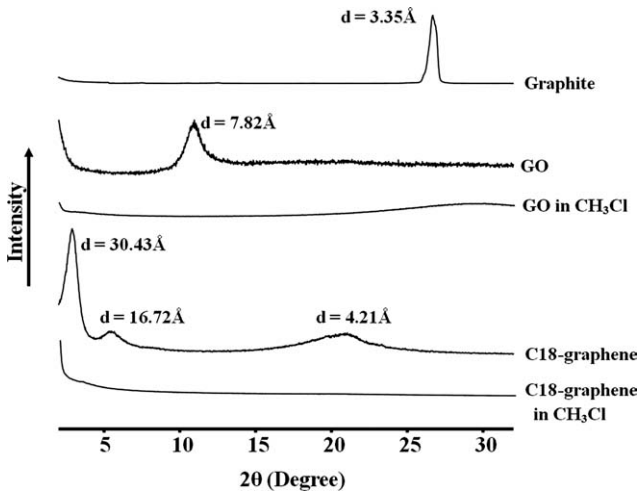

Figure 5 XRD patterns of Graphite, GO, and C18-graphene.

Figure 6(a) shows the dispersed solution of GO/H_2O. The synthesized GO is a black powder while its solution in water appears light brown for concentrations up to 10 mg/mL; above this critical content, gelation occurs. Samulski and coworkers[16] reported that GO can be readily dispersed in water in concentrations up to 2 mg/mL in the pH range 3–10. Ruoff and coworkers[17] also reported that a homogeneous aqueous GO suspension could be obtained with concentrations as high as 7 mg/mL. Our synthesized C18-graphene can be readily dispersed in chloroform with concentrations up to 10 mg/mL without sedimentation; its solution appears colorless and transparent for concentrations below 2 mg/mL, as shown in Figure 6(b).

Figure 7 shows the XRD patterns for pure-ABS and ABS-hybrid films with C18-graphene loadings of 0–3 wt %. For the ABS hybrids with C18-graphene concentrations less than or equal to 2 wt %, no C18-graphene peaks appear in the XRD results, indicating that the C18-graphene in those hybrids produced

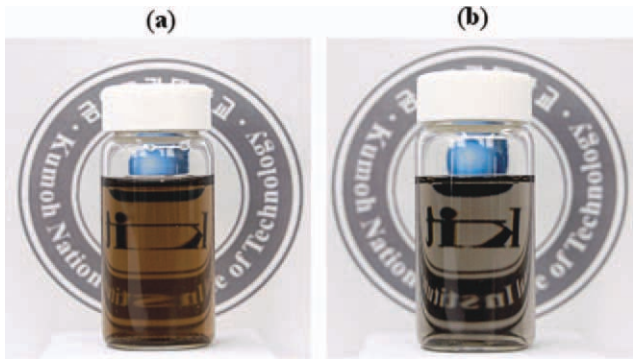

Figure 6 Photographs of dispersion solutions: (a) GO in H_2O and (b) C18-graphene in CH_3Cl. [Color figure can be viewed in the online issue, which is available at wileyonlinelibrary.com.].

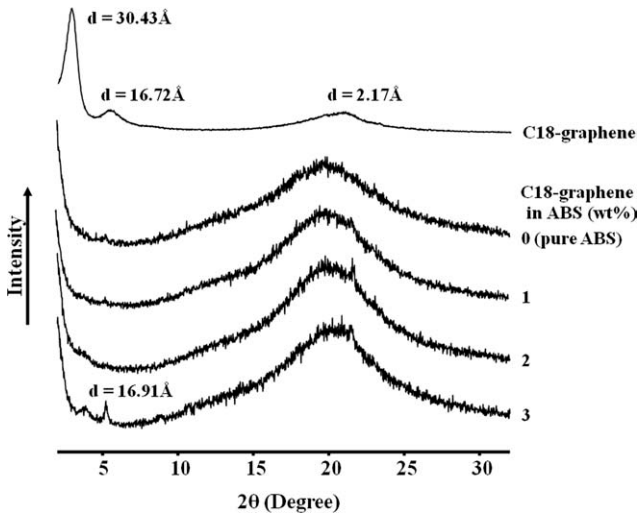

Figure 7 XRD patterns of ABS nanocomposites with various C18-graphene contents.

exfoliated nanocomposites.[18,19] In the case of the hybrid with 3 wt % C18-graphene loading, however, a small peak is observed at $2\theta = 5.22^\circ$ ($d = 16.91$ Å), indicating that agglomeration of a small fraction of the graphene has occurred in the ABS matrix. This suggests that an increase in the extent of graphene aggregation occurs with increasing graphene concentration.[20]

The fracture surfaces of the films were viewed under SEM. Figure 8 shows a comparative analysis of the SEM micrographs for ABS hybrids containing different C18-graphene contents, exhibiting the platelet-orientation distribution morphology. Because of the difference in the scattering densities of the graphene and the matrix polymer, graphene dispersions are readily observed in the SEM images. Figure 8(b–d) show good dispersion of the graphenes in the polymer matrix at all magnification levels. Interestingly, Figure 8(b–d) also show that most of the graphene remains in the form of straight and rigid platelets in the composite, indicating that the graphenes are extremely stiff.

More direct evidence of the formation of a true nanoscale composite was provided by TEM analysis of ultramicrotomed sections of the hybrid films. TEM micrographs of the 1 wt % hybrid film, taken at different magnifications, are shown in Figure 9. The TEM micrographs show that the graphene is dispersed in the polymer matrix at all magnifications, although some graphene agglomerates with sizes greater than ~30 nm are observed. Unlike the hybrids containing 1 wt % C18-graphene, the graphene layers of the 3 wt % hybrid are agglomerated into the matrix polymer (see Fig. 10), which is consistent with the XRD data shown in Figure 7. It is clear that the agglomeration of the dispersed graphene phase increases with increasing graphene

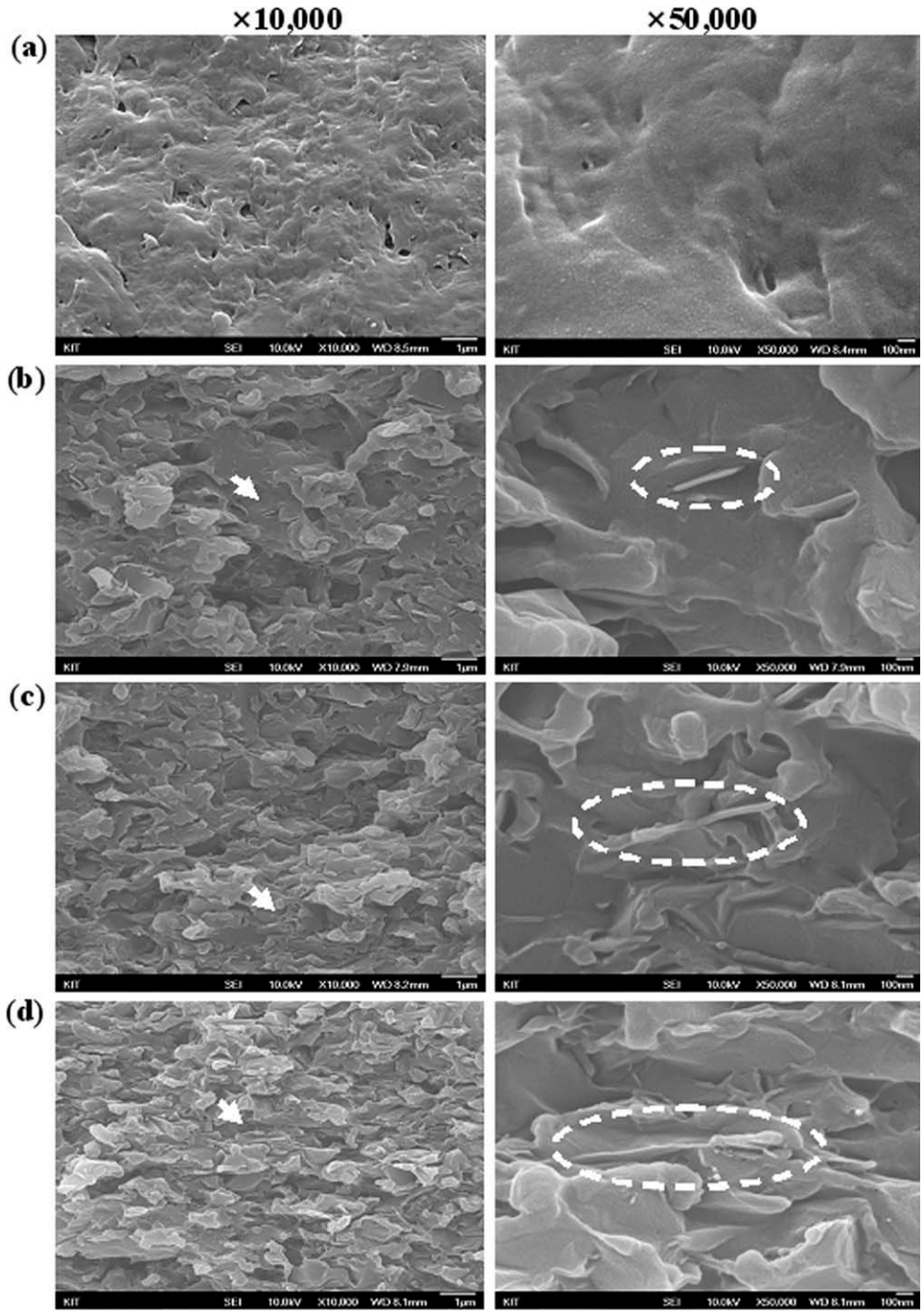

Figure 8 SEM photographs of ABS nanocomposites containing (a) 0 (pure ABS), (b) 1, (c) 2, and (d) 3 wt % C18-graphene at different magnifications (×10,000 and ×50,000).

content. The agglomerated graphene domains may degrade the thermo-mechanical properties of the hybrids because of the poor interfacial adhesion between C18-graphene and the ABS matrix polymer.

Thermal behavior

The thermal properties of ABS-hybrid films with various C18-graphene contents are shown in Table I. The glass transition temperature (T_g) of ABS-hybrid films was found to increase from 94 to 103°C with increasing graphene loading from 0 to 1 wt %. This observed increase in glass transition temperature with graphene addition could be due to several factors,[21] including a corresponding increase in cross-link density and the restriction of the segmental relaxation of the chain segments near the graphene sheets. The glass transition temperature of ABS-hybrid films was found to decrease from 103 to 96°C when the C18-graphene loading in the ABS matrix

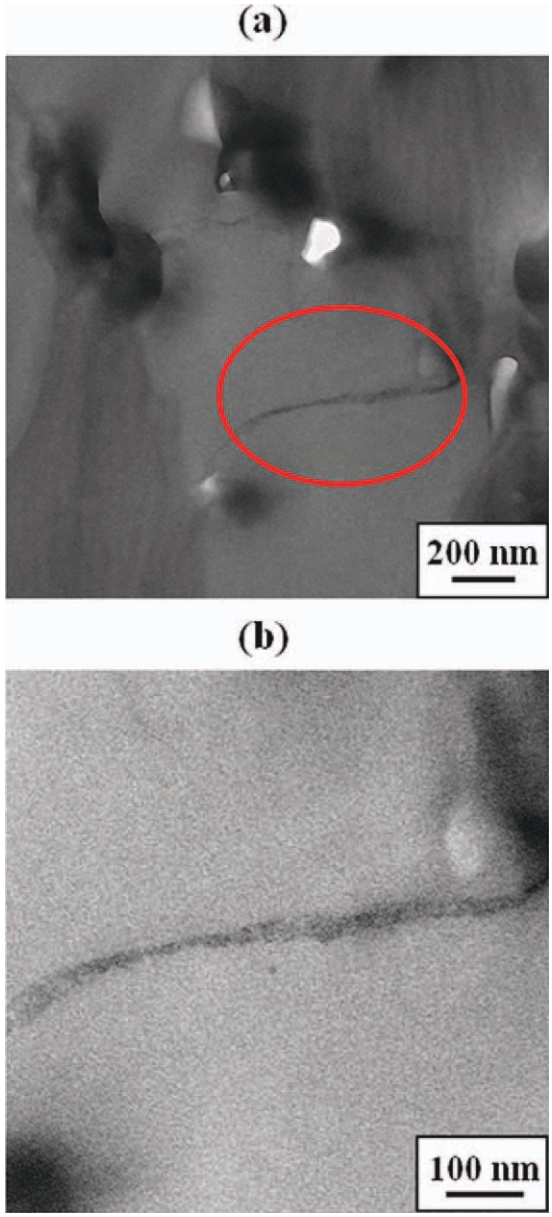

Figure 9 TEM micrographs of 1 wt % C18-graphene in ABS hybrid films increasing the magnification level from (a) to (b). [Color figure can be viewed in the online issue, which is available at wileyonlinelibrary.com.].

was increased from 1 to 3 wt %. This decrease in T_g seems to be the result of graphene agglomeration (see Fig. 7), which occurs with the addition of C18-graphene into the polymer matrix above a critical C18-graphene loading.

The TGA results for the ABS and ABS-hybrid films with various C18-graphene contents are also shown in Table I. A similar trend was found in the initial thermal degradation temperature (T_D^i). The T_D^i at 2% weight loss of the ABS hybrids was found to be in the range 130–160°C for C18-graphene contents of 0–3 wt %, with a maximum increase of 30°C observed in the case of the 1 wt % C18-graphene/ ABS with respect to that of pure ABS. As for the glass transition temperature, this result for T_D^i is probably due to agglomeration of the filler sheets above a critical C18-graphene content. The introduction of filler components into organic polymers can improve their thermal degradation stabilities; graphenes add thermal stability to nanocomposites because of the thermal isolation effect of the graphene sheets and the mass transport barrier they provide to the volatile products generated during thermal decomposition. This kind of improvement in thermal stability has previously been observed in many hybrid systems.[22–24]

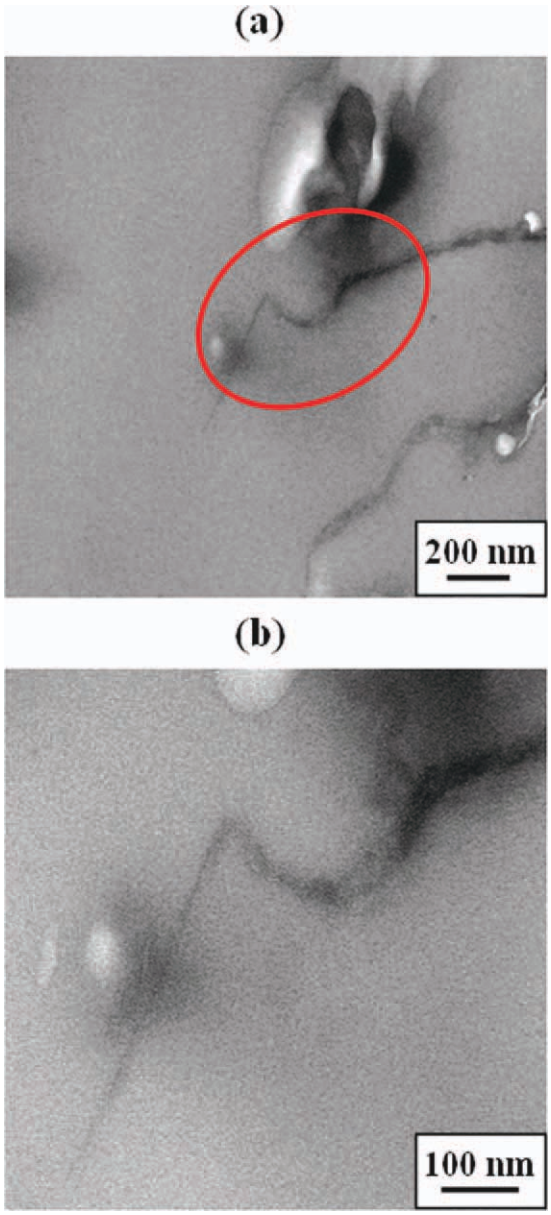

Figure 10 TEM micrographs of 3 wt % C18-graphene in ABS hybrid films increasing the magnification level from (a) to (b). [Color figure can be viewed in the online issue, which is available at wileyonlinelibrary.com.].

For this hybrid system, the largest improvement in the thermal properties was observed for a C18-graphene loading of only 1 wt %. In contrast to the trend in the thermal properties, the weight of the residue at 600°C was found to increase with increasing C18-graphene loadings between 0 and 3 wt %, ranging from 1 to 3% as shown in Table I.

Tensile mechanical properties

The tensile mechanical properties of pure ABS and the hybrid films are shown in Table II. The maximum strength of ABS-hybrid films increases with the addition of C18-graphene up to a critical graphene loading, and then decreases above that critical content, with the greatest strength (29 MPa) observed at a graphene content of 1 wt %. When the C18-graphene content is increased from 1 to 3 wt %, the strength decreases linearly from 29 to 22 MPa, as shown in Table II.

A similar trend is observed for the initial modulus, which increases from 1.45 to 1.72 GPa with increasing C18-graphene content from 0 to 1 wt % and then decreases to 1.60 GPa for 3 wt % C18-graphene content. This decrease in strength and modulus beyond 1 wt % loading is mainly because of the agglomeration of graphene sheets above the critical graphene loading, as previously described.

An increase in the mechanical tensile strength and modulus with inorganic filler is very common for engineering plastics and is usually observed for flexible, coil-like polymers.[25–27] In this hybrid system, however, the reinforcing effect did not obey the rule of mixtures.[21,28] The results presented above indicate that the enhanced mechanical properties of the films containing functionalized-graphene are directly due to the reinforcement provided by the intercalation of ABS in graphene galleries, as well as by the dispersion of graphene sheets in the polymer matrix. The improvements in the tensile mechanical properties also depend on the interactions between the ABS molecules and the layered graphene, as well as on the rigidity of the graphene sheets.[13,29,30]

The elongation at breakage of the hybrid films is found to be virtually unchanged by variations in the graphene content: it varies from 2 to 3% as the C18-graphene content is increased from 0 to 3 wt %. This result is characteristic of materials reinforced with stiff graphene modifiers, as shown in Figure 8.

TABLE I
Thermal Properties of ABS/C18-Graphene Nanocomposite Films

C18-graphene in ABS (wt %)	T_g (°C)	T_D^i (°C)[a]	wt_R^{600} (%)[b]
0 (pure ABS)	94	130	1
1	103	160	2
2	98	153	3
3	96	150	3

[a] At a 2% initial weight-loss temperature.
[b] Weight percent of residue at 600°C.

TABLE II
Mechanical Properties of ABS/C18-Graphene Nanocomposite Films

C18-graphene in ABS (wt %)	Thickness (μm)	Max. str. (MPa)	Ini. mod. (GPa)	E. B. (%)
0 (pure ABS)	132	21	1.45	2
1	102	29	1.72	3
2	93	25	1.70	2
3	99	22	1.60	2

CONCLUSIONS

The AFM, XRD, and SEM results indicate that the C18-graphene was synthesized successfully, and confirm that the C18-graphene is dispersed homogeneously in the ABS matrix. It is found that the addition of only a small amount of functionalized graphene is sufficient to improve the thermal behavior and tensile mechanical properties of ABS-hybrid films, with the maximum enhancement observed at 1 wt % C18-graphene.

References

1. Seyller, T.; Bostwick, A.; Emtsev, K. V.; Horn, K.; Ley, L.; McChesney, J. L.; Ohta, T.; Riley, J. D.; Rotenberg, E.; Speck, F. Phys Stat Sol 2008, 245, 1436.
2. Avouris, P.; Chen, Z.; Perebeinos, V. Nat Nanotechnol 2007, 2, 605.
3. Ghosh, A.; Subrahmanyam, K. S.; Krishna, K. S.; Datta, S.; Govindaraj, A.; Pati, S. K.; Rao, C. N. R. J Phys Chem 2008, 112, 15704.
4. Geim, A. K.; Novoselov, K. S. Nat Mater 2007, 6, 183.
5. Novoselov, K. S.; Geim, A. K.; Morozov, S. V.; Jiang, D.; Zhang, Y.; Dubonos, S. V.; Grigorieva, I. V.; Firsov, A. A. Science 2004, 306, 666.
6. Mattausch, A.; Pankratov, O. Phys Stat Sol 2008, 245, 1425.
7. Xu, Y.; Bai, H.; Lu, G.; Li, C.; Shi, G. J Am Chem Soc 2008, 130, 5856.
8. Li, D.; Müller, M. B.; Gilje, S.; Kaner, R. B.; Wallace, G. G. Nat Nanotechnol 2008, 3, 101.
9. Eda, G.; Fanchini, G.; Chhowalla, M. Nat Nanotechnol 2008, 3, 270.
10. Stankovich, S.; Dikin, D. A.; Dommett, G. H. B.; Kohlhaas, K. M.; Zimney, E. J.; Stach, E. A.; Piner, R. D.; Nguyen, S. T.; Ruoff, R. S. Nature 2006, 442, 282.
11. Hummers, W. S.; Offeman, R. E. J Am Chem Soc 1958, 80, 1339.
12. Matsuo, Y.; Higashika, S.; Kimira, K.; Miyamoto, Y.; Fukutsukab, T.; Sugie, Y. J Mater Chem 2002, 12, 1592.
13. Ansari, S.; Giannelis, E. P. J Polym Sci Part B: Polym Phys 2009, 47, 888.
14. McAllister, M. J.; Li, J. L.; Adamson, D. H.; Schniepp, H. C.; Abdala, A. A.; Liu, J.; Alonso, M. H.; Milius, D. L.; Car, R.; Prud'homme, R. K.; Aksay, I. A. Chem Mater 2007, 19, 4396.
15. Lomeda, J. R.; Doyle, C. D.; Kosynkin, D. V.; Hwang, W. F.; Tour, J. M. J Am Chem Soc 2008, 130, 16201.

16. Si, Y.; Samulski, E. T. Nano Lett 2008, 8, 1679.
17. Park, S.; An, J.; Pinere, R. D.; Jung, I.; Yang, D.; Velamakanni, A.; Nguyen, S. T.; Ruoff, R. S. Chem Mater 2008, 20, 6592.
18. Morgan, A. B.; Gilman, J. W. J Appl Polym Sci 2003, 87, 1329.
19. Eckel, D. F.; Balogh, M. P.; Fasulo, P. D.; Rodgers, W. R. J Appl Polym Sci 2004, 93, 1110.
20. Galgali, G.; Ramesh, C.; Lele, A. Macromolecules 2001, 34, 852.
21. Chang, J. H.; Seo, B. S.; Kim, S. H. J Polym Sci Part B: Polym Phys 2004, 42, 3667.
22. Brown, J. M.; Curliss, D.; Vaia, R. A. Chem Mater 2000, 12, 3376.
23. Xu, H.; Kuo, S. W.; Lee, J. S.; Chang, F. C. Macromolecules 2002, 35, 8788.
24. Park, J. S.; Chang, J. H. Polym Eng Sci 2009, 49, 1357.
25. Lagaly, G. Appl Clay Sci 1999, 15, 1.
26. Giannelis, E. P. Adv Mater 1996, 8, 29.
27. Usuki, A.; Koiwai, A.; Kojima, Y.; Kawasumi, M.; Okada, A.; Kurauchi, T.; Kamigaito, O. J Appl Polym Sci 1995, 5, 119.
28. Weiss, R. A.; Huh, W.; Nicolais, L. Polym Eng Sci 1987, 27, 684.
29. Wang, G.; Wang, B.; Park, J.; Yang, J.; Shen, X.; Yao, J. Carbon 2009, 47, 68.
30. Kuilla, T.; Bhadra, S.; Yao, D.; Kim, N. H.; Bose, S.; Lee, J. H. Prog Polym Sci 2010, 35, 1350.